UNVEILING INVARIANCES VIA NETWORK PRUNING

Anonymous authors
Paper under double-blind review

ABSTRACT

Invariance describes transformations that do not alter data's underlying semantics. Neural networks that preserve natural invariance capture good inductive biases and achieve superior performance. Hence, modern networks are handcrafted around well-known invariances (ex. translations). We propose a framework to learn novel network architectures that capture data-dependent invariances via pruning. Our learned architectures consistently outperform dense neural networks on both vision and tabular datasets in both efficiency and effectiveness. We demonstrate our framework on several neural networks across 3 vision and 40 tabular datasets.

1 INTRODUCTION

Preserving invariance is a key property in successful neural network architectures. Invariance occurs when the semantics of data remains unchanged under a set of transformations (Bronstein et al., 2017). For example, an image of a cat can be translated, rotated, and scaled, without altering its underlying contents. Neural network architectures that represent data passed through invariant transformations with the same representation inherit a good inductive bias (Neyshabur, 2020; 2017; Neyshabur et al., 2014) and achieve superior performance (Zhang et al., 2021; Arpit et al., 2017).

Convolutional Neural Networks (CNNs) are one such example. CNNs achieve translation invariance by operating on local patches of data and weight sharing. Hence, early CNNs outperform large multilayer perceptrons (MLP) in computer vision (LeCun et al., 2015; 1998). Recent computer vision works explore more general spatial invariances, such as rotation and scaling (Satorras et al., 2021; Deng et al., 2021; Delchevalerie et al., 2021; Sabour et al., 2017; Cohen & Welling, 2016; Jaderberg et al., 2015; Qi et al., 2017; Jaderberg et al., 2015; Xu et al., 2014). Other geometric deep learning works extend CNNs to non-Euclidean data by considering more data-specific invariances, such as permutation invariance (Wu et al., 2020; Kipf & Welling, 2016; Defferrard et al., 2016).

Designing invariant neural networks requires substantial human effort: both to determine the set of invariant transformations and to handcraft architectures that preserve said transformations. In addition to being labor-intensive, this approach has not yet succeeded for all data-types (Schäfl et al., 2022; Gorishniy et al., 2022; 2021; Huang et al., 2020). For example, designing neural architectures for tabular data is especially hard because the set of invariant tabular transformations is not clearly-defined. Thus, the state-of-the-art deep learning architecture on tabular data remains highly tuned MLPs (Kadra et al., 2021; Grinsztajn et al., 2022; Gorishniy et al., 2022).

Existing invariance learning methods operate at the data augmentation level (Immer et al., 2022; Quiroga et al., 2020; Benton et al., 2020; Cubuk et al., 2018), where a model is trained on sets of transformed samples rather than individual samples. This makes the network resiliant to invariant transformations at test time. Contrastive learning (CL) is a possible means of incorporating invariance (Dangovski et al., 2021), and has seen success across various tasks (Chen et al., 2021; Zhu et al., 2021; You et al., 2020b; Jaiswal et al., 2020; Baevski et al., 2020; Chen et al., 2020), including tabular learning (Bahri et al., 2021). While these approaches train model parameters to capture new data-dependent invariances, the model architecture itself still suffers from a weak inductive bias.

In contrast, existing network pruning works found shallow MLPs can automatically be compressed into sparse subnetworks with good inductive bias by pruning the MLP itself (Neyshabur, 2020). Combining pruning and invariance learning has largely been unsuccessful (Corti et al., 2022). Furthermore, pruning for invariance does not scale to deep MLPs, possibly due to issues in the lazy training regime (Tzen & Raginsky, 2020; Chizat et al., 2019) where performance improves yet

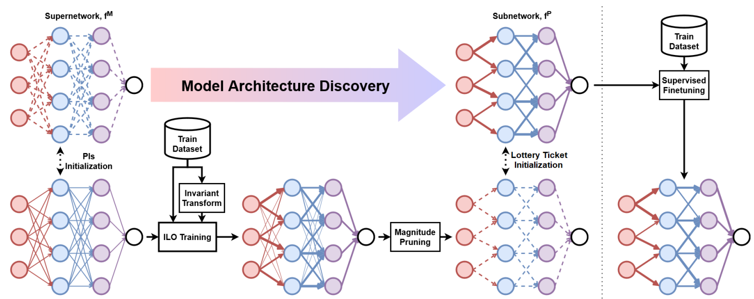

Figure 1: Overview for the IUNET Framework. The supernetwork, $f^P(\cdot;\theta_M)$, is initialized using PIs and trained on the ILO objective to obtain $\theta_M^{(T)}$. Magnitude-based pruning is used to get a new architecture $f^P = \mathcal{P}(\theta_M^{(T)})$. The new architecture, $f^P(\cdot;\theta_P)$, is initialized via lottery ticket reinitialization and finetuned with supervised maximum likelihood loss.

weights magnitudes stay near static over training. Combining invariance learning with network pruning remains an open question.

We propose **I**nvariance **U**nveiling Neural **Net**works, IUNET, a pruning framework that discovers invariance-preserving subnetworks from deep and dense supernetworks. We hypothesize pruning for invariance fails on deep networks due to the lazy training issue (Liu et al., 2023), where performance decouples from weight magnitudes. We address this with a proactive initialization scheme (PIS), which prevents important weights from being pruned through encouraging almost all weights to be near zero. To capture useful invariances, we propose a novel invariance learning objective (ILO), that successfully combines CL with network pruning by regularizing it with maximum likelihood.

To the best of our knowledge, we are the first to automatically design deep architectures that incorporate invariance using pruning. We summarize our contributions below:

- Designing architectures from scratch is difficult when desired invariances are hard to incorporate. We automatically discover an invariance-preserving subnetwork that outperforms an invariance-agnostic supernetwork on both vision and tabular data.
- Network pruning is used to compress models for mobile devices. Our approach consistently improves compression performance for existing vision and tabular models.
- Contrastive learning traditionally fails when combined with network pruning. We are the first to successfully combine contrastive learning with network pruning by regularizing it with our simple yet effective invariance learning objective.
- In the lazy training regime, performance improves drastically while weight magnitudes stay relatively constant, hence a weight's importance to downstream performance is decoupled from its magnitude. We provide an effective approach that encourages only important weights to have large magnitudes before the lazy training regime begins.

2 Related Work

2.1 Learning Invariances

Most invariant networks are handcrafted to capture specific spatial invariances (Dehmamy et al., 2021; Satorras et al., 2021; Deng et al., 2021; Qi et al., 2017; Vaswani et al., 2017; Cohen & Welling, 2016; Kipf & Welling, 2016; Jaderberg et al., 2015; LeCun et al., 1998). Learning invariance usually involves data augmentation followed by ensembling. (Immer et al., 2022; Quiroga et al., 2020; Lorraine et al., 2020; Benton et al., 2020; Cubuk et al., 2018). Some works use meta-learning to incorporate parameter sharing into a given architecture (Zhou et al., 2020; Kirsch et al., 2022). None of the aforementioned works generates architectures from scratch to improve the network's inductive bias. The closest work is β-LASSO (Neyshabur, 2020) which discovers shallow subnetworks with local connectivity through pruning for computer vision. Our work extends this idea to deeper networks and explores the tabular data setting.

Dataset	MLP_{VIS}	OMP $^{(\text{MLP}_{\text{VIS}})}$	β-LASSO $^{(\text{MLP}_{\text{VIS}})}$	IUNET $^{(\text{MLP}_{\text{VIS}})}$
CIFAR10	59.266 ± 0.050	59.668 ± 0.171	59.349 ± 0.174	$\mathbf{64.847 \pm 0.121}$
CIFAR100	31.052 ± 0.371	31.962 ± 0.113	31.234 ± 0.354	$\mathbf{32.760 \pm 0.288}$
SVHN	84.463 ± 0.393	85.626 ± 0.026	84.597 ± 0.399	$\mathbf{89.357 \pm 0.156}$

Dataset	RESNET	OMP $^{(\text{RESNET})}$	β-LASSO $^{(\text{RESNET})}$	IUNET $^{(\text{RESNET})}$
CIFAR10	73.939 ± 0.152	75.419 ± 0.290	74.166 ± 0.033	$\mathbf{83.729 \pm 0.153}$
CIFAR100	42.794 ± 0.133	44.014 ± 0.163	42.830 ± 0.412	$\mathbf{53.099 \pm 0.243}$
SVHN	90.235 ± 0.127	90.474 ± 0.192	90.025 ± 0.201	$\mathbf{94.020 \pm 0.291}$

Table 1: Comparing different pruning approaches to improve the inductive bias of MLP_{VIS} and RESNET on computer vision datasets. Notice, IUNET performs substantially better than existing pruning-based methods by discovering novel architectures that better capture the inductive bias. IUNET flexibly boosts performance of off-the-shelf models.

Metric	MLP_{TAB}	OMP	β-LASSO	IUNET	XGB	TABN	$\text{MLP}_{\text{TAB+C}}$
Num Top1 ↑	1	4	1	13	12	0	**16**
Average Acc ↑	82.644	82.401	82.516	**83.046**	80.534	74.383	82.922
Average Rank ↓	3.988	3.975	4.087	3.225	3.813	6.325	**2.588**

Table 2: We report the number of datasets out of 40 where each method was best, the average accuracy achieved by each method, and the average ranking of each method. OMP, β-LASSO, and IUNET all modify MLP_{TAB}. $\text{MLP}_{\text{TAB+C}}$ performed substantially more hyperparameter tuning than than IUNET. For full results, please refer to the Appendix.

2.2 NEURAL NETWORK PRUNING

Neural network pruning compresses large supernetworks without hurting performance (Frankle & Carbin, 2018; Louizos et al., 2017). A pinnacle work is the Lottery Ticket Hypothesis (LTH) (Frankle & Carbin, 2018; Liu et al., 2018b; Blalock et al., 2020), where pruned networks can retain unpruned peformance when reinitialized to the start of training and iteratively retrained. One-Shot Magnitude Pruning (OMP) studies how to prune the network only once (Blalock et al., 2020). The lazy training regime (Chizat et al., 2019) is a possible bottleneck for network pruning (Liu et al., 2023). Contrastive learning does not work with network pruning (Corti et al., 2022). Recent pruning policies improve efficiency by starting with a sparse network (Evci et al., 2020). or performing data-agnostic Zero-Shot Pruning (Hoang et al., 2023; Wang et al., 2020; Lee et al., 2019). Interestingly, subnetworks rarely outperform the original supernetwork, which has been dubbed the “Jackpot” problem (Ma et al., 2021). In contrast to existing works, we successfully combine OMP with contrastive learning, alleviate the lazy learning issue, and outperform the original supernetwork.

3 PROPOSED METHOD: IUNET

3.1 PROBLEM SETTING

We study the classification task with inputs, $x \in \mathcal{X}$, class labels, $y \in \mathcal{Y}$, and hidden representations, $h \in \mathcal{H}$. Our neural network architecture, $f(x;\theta) : \mathcal{X} \to \mathcal{Y}$ is composed of an encoder, $f_{\mathcal{E}}(\cdot;\theta) : \mathcal{X} \to \mathcal{H}$ and decoder, $f_{\mathcal{D}}(\cdot;\theta) : \mathcal{H} \to \mathcal{Y}$, where $\theta \in \Theta$ are the weights and $f = f_{\mathcal{E}} \circ f_{\mathcal{D}}$. During training, we denote the weights after $0 < t < T$ iterations of stochastic gradient descent as $\theta^{(t)}$.

First, we define our notion of invariance. Given a set of invariant transformations, $\mathcal{S}$, we wish to discover a neural network architecture $f^*(x;\theta)$, such that all invariant input transformations map to the same representation, shown in Equation 1. We highlight our task focuses on the discovery of novel architectures, $f^*(\cdot;\theta)$, not weights, θ, because improved architectures capture better inductive bias, which ultimately improves downstream performance (Neyshabur, 2017).

$$f^*_{\mathcal{E}}(x;\theta) = f^*_{\mathcal{E}}(g(x);\theta), \forall g \in \mathcal{S}, \forall \theta \in \Theta. \tag{1}$$

Dataset	$g(\cdot)$	MLP_{VIS}	IUNET $^{(\text{MLP}_{\text{VIS}})}$
CIFAR10	resize.	44.096 ± 0.434	$\mathbf{97.349 \pm 4.590}$
	horiz.	80.485 ± 0.504	$\mathbf{99.413 \pm 1.016}$
	color.	56.075 ± 0.433	$\mathbf{98.233 \pm 3.060}$
	graysc.	81.932 ± 0.233	$\mathbf{99.077 \pm 1.598}$

Dataset	$g(\cdot)$	MLP_{TAB}	IUNET $^{(\text{MLP}_{\text{TAB}})}$
mfeat.	feat.	46.093 ± 1.353	$\mathbf{51.649 \pm 4.282}$

Table 3: Comparing the consistency metric (%) of the untrained supernetwork, MLP_{VIS} and MLP_{TAB}, against IUNET's pruned subnetwork under different invariant transforms, $g(\cdot)$. IUNET preserves invariances better.

3.2 Framework

We accomplish this by first training a dense supernetwork, $f^M(\cdot;\theta_M)$, with enough representational capacity to capture the desired invariance properties, as shown in Equation 2. A natural choice for $f^M(\cdot;\theta_M)$ is a deep MLP, which is a universal approximator (Cybenko, 1989).

$$\exists \theta_M^* \in \Theta_M : f_{\mathcal{E}}^M(x;\theta_M^*) = f_{\mathcal{E}}^M(g(x);\theta_M^*), \forall g \in \mathcal{S}. \tag{2}$$

Next, we initialize the supernetwork's weights, $\theta_M^{(0)}$, using our Proactive Initialization Scheme, PIS, and train the supernetwork with our Invariance Learning Objective, ILO, to obtain $\theta_M^{(T)}$. We discuss both PIS's and ILO's details in following sections.

We construct our new untrained subnetwork, $f^P(\cdot;\theta_P^{(0)})$, from the trained supernetwork, $f^M(\cdot;\theta_M^{(T)})$, where the subnetwork contains a subset of the supernetwork's weights, $\theta_P^{(0)} \subset \theta_M^{(T)}$ and $|\theta_P^{(0)}| \ll |\theta_M^{(T)}|$, and is architecturally different from the supernetwork, $f^P(\cdot;\cdot) \neq f^M(\cdot;\cdot)$. For this step, we adopt standard One-shot Magnitude-based Pruning (OMP), where the smallest magnitude weights and their connections in the supernetwork architecture are dropped. We adopt OMP because of its success in neural network pruning (Frankle & Carbin, 2018; Blalock et al., 2020). We represent this step as an operator mapping supernetwork weights into subnetwork architectures $\mathcal{P} : \Theta_M \to \mathcal{F}_P$, where $\mathcal{F}_P$ denotes the space of subnetwork architectures.

$$f_{\mathcal{E}}^{P*}(x;\theta_{P*}) = f_{\mathcal{E}}^{P*}(g(x);\theta_{P*}), \forall g \in \mathcal{S}, \forall \theta_{P*} \in \Theta_{P*} \tag{3}$$

Finally, we re-initialize the subnetwork's weights, $\theta_P^{(0)}$, using the Lottery Ticket Re-initialization scheme (Frankle & Carbin, 2018) then finetune the subnetwork with maximum likelihood to obtain $\theta_P^{(T)}$. We hypothesize the trained subnetwork, $f^P(\cdot;\theta_P^{(T)})$, can outperform the trained original supernetwork, $f^M(\cdot;\theta_M^{(T)})$, if it preserves desired invariances and hence improves the inductive bias. The ideal subnetwork, $f^{P*}(\cdot;\theta_{P*})$, preserves invariances even without training, as shown in Equation 3.

We call this framework, including the ILO loss and PIS initialization, IUNET[1], as shown in Figure 1

3.2.1 Invariance Learning Objective: ILO

The goal of supernetwork training is to create a subnetwork, $f^P(\cdot;\theta_P^{(0)})$, within the supernetwork, $f^M(\cdot;\theta_M^{(T)})$, such that:

1. $\mathcal{P}(\theta_M^{(T)})$ achieves superior performance on the classification task after finetuning.
2. $\mathcal{P}(\theta_M^{(T)})$ captures desirable invariance properties as given by Equation 3.
3. $\theta_P^{(0)}$ has higher weight values than $\theta_M^{(T)} \setminus \theta_P^{(0)}$.

Dataset	MLP_{VIS}	IUNET $^{(\text{MLP}_{\text{VIS}})}_{\text{NO-PRUNE}}$	IUNET $^{(\text{MLP}_{\text{VIS}})}_{\text{NO-ILO}}$	IUNET $^{(\text{MLP}_{\text{VIS}})}_{\text{NO-PIS}}$	IUNET $^{(\text{MLP}_{\text{VIS}})}$
CIFAR10	59.266	54.622 ± 0.378	62.662 ± 0.169	60.875 ± 0.292	$\mathbf{64.847 \pm 0.121}$
CIFAR100	31.052	20.332 ± 0.065	32.242 ± 0.321	32.747 ± 0.346	$\mathbf{32.760 \pm 0.288}$
SVHN	84.463	78.427 ± 0.683	88.870 ± 0.139	85.247 ± 0.071	$\mathbf{89.357 \pm 0.156}$

Dataset	MLP_{TAB}	IUNET $^{(\text{MLP}_{\text{TAB}})}_{\text{NO-PRUNE}}$	IUNET $^{(\text{MLP}_{\text{TAB}})}_{\text{NO-ILO}}$	IUNET $^{(\text{MLP}_{\text{TAB}})}_{\text{NO-PIS}}$	IUNET $^{(\text{MLP}_{\text{TAB}})}$
arrhythmia	67.086	56.780 ± 6.406	71.385 ± 6.427	$\mathbf{78.675 \pm 7.078}$	74.138 ± 2.769
mfeat.	98.169	97.528 ± 0.400	$\mathbf{98.471 \pm 0.344}$	98.339 ± 0.203	98.176 ± 0.121
vehicle	80.427	80.427 ± 1.806	81.411 ± 0.386	80.928 ± 0.861	$\mathbf{81.805 \pm 2.065}$
kc1	80.762	$\mathbf{84.597 \pm 0.000}$	82.456 ± 1.850	$\mathbf{84.597 \pm 0.000}$	$\mathbf{84.597 \pm 0.000}$

Table 4: Ablation Study on vision and tabular datasets.

Because subnetworks pruned from randomly initialized weights, $\mathcal{P}(\theta_M^{(0)})$, are random, they include harmful inductive biases that hinders training. Thus, we optimize the trained supernetwork, $f^M(\cdot;\theta_M^{(T)})$, on goals (1) and (2) as a surrogate training objective. Goal (3) is handled by PIS, described in the next section.

To achieve (1), we maximize the log likelihood of training data. To achieve (2), we minimize the distance between representations of inputs under invariant perturbations, stated in Equation 5. Intuitively, achieving (2) entails optimizing the supernetwork in metric space, which we find is equivalent to Supervised Contrastive Learning (SCL) as state in Theorem 1.[2]

Theorem 1 *Minimizing the distance between representations of inputs under a set of invariant perturbations, Equation 4, is equivalent to minimizing the supervised contrastive learning objective, Equation 5, where $f_{\mathcal{E}}^M : \mathbb{R} \to \mathbb{R}^d$ is a supernetwork, $\psi^{(cos)} : \mathbb{R}^d \times \mathbb{R}^d \to \mathbb{R}$ is cosine similarity, $\phi : \mathbb{R}^d \times \mathbb{R}^d \to \mathbb{R}$ is a distance metric, and $g : \mathcal{X} \to \mathcal{X}$ is a desired invariance function from $\mathcal{S}$.*

$$\theta_M^* = \underset{\theta_M}{argmax} \underset{\substack{x_i, x_j \sim \mathcal{X} \\ g \sim \mathcal{S}}}{\mathbb{E}} \left[\frac{\phi(f_{\mathcal{E}}^M(x_i;\theta_M), f_{\mathcal{E}}^M(x_j;\theta_M))}{\phi(f_{\mathcal{E}}^M(x_i;\theta_M), f_{\mathcal{E}}^M(g(x_i);\theta_M))} \right] \tag{4}$$

$$= \underset{\theta_M}{argmin} \underset{\substack{x, y \sim D_{tr} \\ g \sim \mathcal{S}}}{\mathbb{E}} \left[-log \left(\frac{exp\left(\psi^{(cos)}\left(f_{\mathcal{E}}^M(x;\theta_M), f_{\mathcal{E}}^M(g(x);\theta_M)\right)\right)}{\sum\limits_{\substack{x', y' \sim D_{tr} \\ y' \neq y}} exp\left(\psi^{(cos)}\left(f_{\mathcal{E}}^M(x;\theta_M), f_{\mathcal{E}}^M(g(x');\theta_M)\right)\right)} \right) \right] \tag{5}$$

Explicitly optimizing both (1) and (2) is necessary for IUNET. Because maximum likelihood on its own does not consider desired invariance properties, pruning will not improve the inductive bias of supernetworks trained solely to optimize (1). For this reason, performance degradation is commonly observed amongst almost all existing pruning algorithms (Hooker et al., 2019; Blalock et al., 2020; Ma et al., 2021). Because pruning already causes the supernetwork to "selectively forget" training samples disproportionately (Hooker et al., 2019) and supernetworks trained solely with contrastive learning amplifies this effect (Corti et al., 2022), pruning will not improve performance of supernetworks trained solely to optimize (2). One reason why contrastive learning amplifies "selective forgetting" is because models overfit constrastive objectives (Zhang et al., 2020; Pasad et al., 2021).

By optimizing both (1) and (2), IUNET uses pruning to enhance the supernetwork by encoding helpful inductive biases into the pruned subnetwork while avoiding overfitting of the contrastive objective. The Invariance Learning Objective (ILO) is shown in Equation 7, where $\mathcal{L}_{NCE}$ is the contrastive loss defined in Equation 5, $\mathcal{L}_{SUP}$ is maximum likelihood loss, D_{tr} is a labelled training dataset of (x, y) pairs, and λ is a hyperparameter.

[1] IUNET prunes an ineffective supernetwork into an efficient effective subnetwork. OMP prunes an inefficient effective supernetwork into an efficient but slightly less effective subnetwork.

[2] Proof of Theorem 1 provided in Appendix.

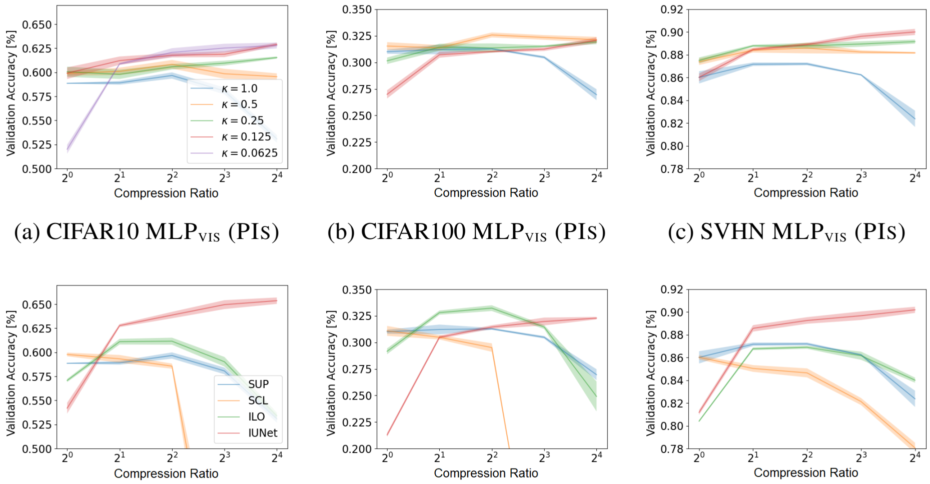

(a) CIFAR10 MLP_{VIS} (PIs) (b) CIFAR100 MLP_{VIS} (PIs) (c) SVHN MLP_{VIS} (PIs)

(d) CIFAR10 MLP_{VIS} (ILO) (e) CIFAR100 MLP_{VIS} (ILO) (f) SVHN MLP_{VIS} (ILO)

Figure 2: Effect of PIs and ILO on pruned models. The y-axis is the validation accuracy (%) and x-axis is the compression ratio. PIs experiments only alter the supernetwork's initialization. $\kappa = 1.0$ means normal initialization. ILO experiments only alter the training objective during supernetwork training. After supernetwork training, subnetworks are pruned under different compression ratios, then finetuned. Validation accuracy of trained pruned models are reported.

$$\mathcal{L}(\theta_M; \mathcal{S}) = \mathop{\mathbb{E}}_{x,y \sim D_{tr}} [\mathcal{L}_{SUP}(x, y, \theta_M) + \lambda \mathcal{L}_{NCE}(x, y, \theta_M; \mathcal{S})] \tag{6}$$

3.2.2 Proactive Initialization Scheme: PIs

Deep neural networks often enter the lazy training regime (Chizat et al., 2019; Liu et al., 2023), where the loss steadily decreases while weights barely change. This is particularly harmful to neural networks pruning (Liu et al., 2023), especially when low-magnitude weights contribute to decreasing the loss and hence should not be pruned.

We propose a simple solution by scaling the weight initialization by a small multiplier, κ. We find this alleviates the aforementioned issue by forcing the model to assign large values only to important weights prior to lazy training. Because lazy training is only an issue for pruning, we only apply κ-scaling to the pre-pruning training stage, not the fine-tuning stage. This is done by scaling the initial weights $\theta_M^{(0)} = \kappa \theta_{M^\dagger}^{(0)}$, where $\theta_{M^\dagger}^{(0)}$ follows the Kaiming (He et al., 2015) or Glorot (Glorot & Bengio, 2010) initialization.

4 Experiment Setup

4.1 Datasets

IUNet is evaluated on *image* and *tabular* classification [3]:

- **Vision**: Experiments are run on CIFAR10, CIFAR100, and SVHN (Krizhevsky et al., 2009; Netzer et al., 2011), following baseline work (Neyshabur, 2020)[4].
- **Tabular**: Experiments are run on 40 tabular datasets from a benchmark paper (Kadra et al., 2021), covering a diverse range of problems. The datasets were collected from OpenML (Gijsbers et al., 2019), UCI (Asuncion & Newman, 2007), and Kaggle.

[3] More details are provided in the Supplementary.

[4] While SMC benchmark (Liu et al., 2023) is open-sourced, the code is being cleaned-up at submission time.

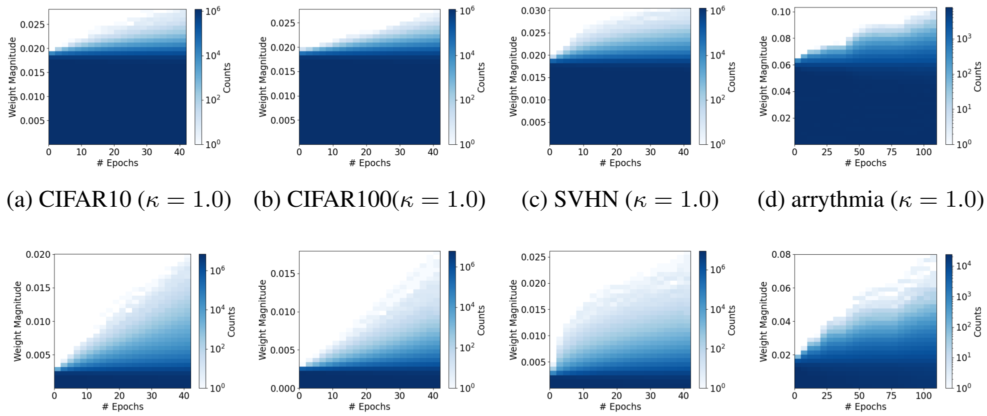

(a) CIFAR10 ($\kappa = 1.0$) (b) CIFAR100($\kappa = 1.0$) (c) SVHN ($\kappa = 1.0$) (d) arrythmia ($\kappa = 1.0$)

(e) CIFAR10 ($\kappa = .125$) (f) CIFAR100($\kappa = .125$) (g) SVHN ($\kappa = .125$) (h) arrythmia ($\kappa = .25$)

Figure 3: Histogram of weight magnitudes, $|\theta_M^{(t)}|$, plotted over each epoch under different κ initializations settings. $\kappa = 1.0$ means normal initialization. Results shown for MLP_{VIS} on the CIFAR10, CIFAR100, and SVHN datasets.

4.2 Model Setup

IUNet is compared against One-shot Magnitude Pruning (OMP) (Blalock et al., 2020), and β-Lasso pruning (Neyshabur, 2020) on all datasets. We denote the supernetwork used by each pruning method with a superscript. Unless otherwise specified, models are trained via maximum likelihood. In addition, we compare against the following dataset-specific supernetworks (MLP_{VIS}, MLP_{TAB}, ResNet) and models:

- **Vision**: We consider ResNet (He et al., 2016), MLP_{VIS}, a MLP that contains a CNN subnetwork (Neyshabur, 2020), and the aforementioned CNN subnetwork.
- **Tabular**: We consider MLP_{TAB}, a 9-layer MLP with hidden dimension 512 (Kadra et al., 2021), XGB (Chen & Guestrin, 2016), TabN (Arik & Pfister, 2021), a handcrafted tabular deep learning architecture, and $\text{MLP}_{\text{TAB+C}}$ (Kadra et al., 2021), the state-of-the-art MLP, which was heavily tuned from a cocktail of regularization techniques.

4.3 Considered Invariances

The success of contrastive learning on both vision and tabular datasets indicates their corresponding invariant transformations, $\mathcal{S}$, are desirable for each task. For computer vision, SimCLR (Chen et al., 2020) transformations are used: (1) resize crops, (2) horizontal flips, (3) color jitter, and (4) random grayscale. For tabular learning, SCARF (Bahri et al., 2021) transformations are used: (5) randomly corrupting features by drawing the corrupted versions from its empirical marginal distribution.

5 Results

5.1 On Inductive Bias

In this section, we compare the effectiveness of the trained subnetwork discovered by IUNet, $f^P(\cdot; \theta_P^{(T)})$, against the trained supernetwork, $f^M(\cdot; \theta_M^{(T)})$. As seen in Tables 1 and 7, the pruned subnetwork outperforms the original supernetwork, even though the supernetwork has more representational capacity. This supports our claim that IUNet prunes subnetwork architectures with better inductive biases than the supernetwork. Importantly, IUNet substantially improves upon existing pruning baselines by explicitly including invariances via ILO and alleviating the lazy learning issue (Liu et al., 2023) via PIs.

On *vision* datasets: As seen in Table 1, IUNET is a general and flexible framework that improves the inductive bias of not only models like MLP_{VIS} but also specialized architectures like RESNET. Specifcally, IUNET $^{(\text{MLP}_{\text{VIS}})}$ bridges the gap between MLPs and CNNs. Unlike previous work (Tolstikhin et al., 2021), IUNET $^{(\text{MLP}_{\text{VIS}})}$ does this in an entirely automated procedure. IUNET $^{(\text{RESNET})}$ achieves the best performance, indicating IUNET can be applied across various models.

On *tabular* datasets: As seen in Table 2, the subnetworks derived from MLPs outperform both the original MLP_{TAB} and hand-crafted architectures: TABN and XGB. Unlike vision, how to encode invariances for tabular data is highly nontrivial, making IUNET particularly effective. The gains made by MLP_{TAB} is similar to those from $\text{MLP}_{\text{TAB+C}}$ (Kadra et al., 2021), which ran extensive hyperparameter tuning on top of MLP_{TAB}. Unlike $\text{MLP}_{\text{TAB+C}}$, IUNET requires substantially less time tuning hyperparameters. Note, IUNET $^{(\text{MLP}_{\text{TAB}})}$ did not use the optimal hyperparameters found by $\text{MLP}_{\text{TAB+C}}$. Furthermore, because IUNET is a flexible framework, it can be combined with new models/ trainig techniques on tabular data as they are discovered.

5.2 ABLATION STUDY

To study the effectiveness of (1) pruning, (2) PIS, and (3) ILO, each one is removed from the optimal model. As seen in Table 4, each is crucial to IUNET. Pruning is necessary to encode the inductive bias into the subnetwork's neural architecture. PIS and ILO improves the pruning policy by ensuring weights crucial to finetuning and capturing invariance are not pruned. Notice, without pruning, IUNET $_{\text{NO-PRUNE}}$ performs worse than the original supernetwork. This highlights an important notion that PIS aims to improve the pruning policy, not the unpruned performance. By sacrificing unpruned performance, PIS ensures important weights are not falsely pruned. PIS is less effective on tabular datasets where the false pruning issue seems less severe. Combining pruning, ILO, and PIS, IUNET most consistently achieves the best performance.

5.3 EFFECTS OF PRUNING

To further study the effects of pruning, we plot how performance changes over different compression ratios. Figure 2 clearly identifies how PIS and ILO substantially improves upon existing pruning policies. First, our results support existing findings that (1) OMP does not produce subnetworks that substantially outperform the supernetwork (Blalock et al., 2020) and (2) while unpruned models trained with SCL can outperform supervised ones, pruned models trained with SCL perform substantially worse (Corti et al., 2022). PIS flips the trend from (1) by slightly sacrificing unpruned performance, due to poorer initialization, IUNET discovers pruned models with better inductive biases, which improves downstream performance. ILO fixes the poor performance of SCL in (2) by preserving information pathways for both invariance and max likelihood over training. We highlight both these findings are significant among the network pruning community. Finally, Figure 2 confirms IUNET achieves the best performance by combining both PIS and ILO.

In addition to being more effective that the supernetwork, $f^M(\cdot;\theta_M^{(T)})$, the pruned network, $f^P(\cdot;\theta_P^{(T)})$, is also more efficient. Figure 2 shows IUNET can reach 8-16$\times$ compression while still keeping superior performance.

5.4 EFFECT OF PROACTIVE INITIALIZATION

To further study the role of PIS, the histogram of weight magnitudes is monitored over the course of training. As shown in Figure 3, under the standard OMP pruning setup, the histogram changes little over the course of training, which supports the lazy training hypothesis (Liu et al., 2023) where performance rapidly improves, while weight magnitudes change very little, decoupling each weight's importance from its magnitude.

With PIS, only important weights grow over the course of training, while most weights remain near zero, barely affecting the output activations of each layer. This phenomenon alleviates the lazy training problem by ensuring (1) pruning safety, as pruned weights are near zero prior which have minimal affect on layer activations, and (2) importance-magnitude coupling, as structurally important connections must grow to affect the output of the layer.

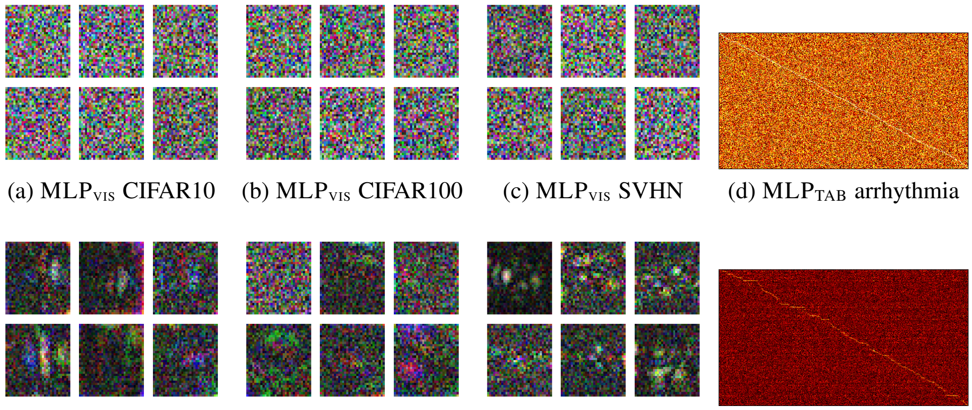

(a) MLP_{VIS} CIFAR10 (b) MLP_{VIS} CIFAR100 (c) MLP_{VIS} SVHN (d) MLP_{TAB} arrhythmia

(e) IUNET CIFAR10 (f) IUNET CIFAR100 (g) IUNET SVHN (h) IUNET arrhythmia

Figure 4: Visualization of weight magnitudes, $|\theta_M^{(T)}|$, trained with different policies. The top row was trained on CIFAR10 and shows the magnitude of each RGB pixel for 6 output logits. The bottom row was trained on arrhythmia and shows the weight matrix of the 1st layer with 280 input and 512 output dimensions. Lighter color means larger magnitude.

5.5 On Invariance Consistency

To further study whether particular invariances are learned, we compute the consistency metric (Singla et al., 2021), which measure the percentage of samples whose predicted label would flip when an invariant transformation is applied to the input. As seen in Table 3, the subnetwork found by IUNET, $f^P(\cdot;\theta_P^{(0)})$, is able to preserve invariances specified in ILO much better than the supernetwork, $f^M(\cdot;\theta_M^{(0)})$. This shows IUNET indeed captures desirable invariances.

5.6 On Weight Visualization

We visualize the supernetwork weights, $\theta_M^{(T)}$, when trained with IUNET compared to standard maximum likelihood (MLP) to determine what structures preserve invariance.

On *vision* datasets: As seen in Figure 4, IUNET learns more locally connected structures, which improves translation invariance. Prior work (Neyshabur, 2020) found network structure (as opposed to inductive bias) to be the limiting factor for encoding CNN inductive biases into MLPs, which IUNET successfully replicates.

On *tabular* datasets: As seen in Figure 4, IUNET weights focus more on singular features. This preserves invariance over random feature corruption, as the absence of some tabular features does not greatly alter output activations of most neurons. This structure can also be likened to tree ensembles (Grinsztajn et al., 2022), whose leaves split individual features rather than all features.

6 Conclusion

In this work, we study the viability of network pruning for discovering invariant-preserving architectures. Under the computer vision setting, IUNET bridges the gap between deep MLPs and deep CNNs, and reliably boosts RESNET performance. Under the tabular setting, IUNET reliably boosts performance of existing MLPs, comparable to applying the state-of-the-art regularization cocktails. Our proposed novelties, ILO and PIS, flexibly improves existing OMP pruning policies by both successfully integrating contrastive learning and alleviating lazy training. Thus, IUNET effectively uses pruning to tackle invariance learning.

7 Reproducibility Statement

We provide a complete description of the data processing steps in Section 4.1 and Appendix E.1. We cover hyperparameters used in Section 4.2, Section 4.3, Appendix E.2, and Appendix E.3. We cover pruning implementation details in Appendix E.4. We cover hardware and approximate runtime in Appendix E.5. The proof for Theorem 1 can be found in Appendix B.1.

8 Ethics Statement

There are no new datasets released by this work, hence it did not involve human subjects. Datasets used in this work were adopted from existing benchmarks (Neyshabur, 2020; Blalock et al., 2020; Kadra et al., 2021), as described in Section 4.1 and Appendix E.1. There are no harms introduced by this work. This work aims to improve both effectiveness and efficiency of representation learning.

References

Sercan Ö Arik and Tomas Pfister. Tabnet: Attentive interpretable tabular learning. In *Proceedings of the AAAI conference on artificial intelligence*, volume 35, pp. 6679–6687, 2021.

Devansh Arpit, Stanisław Jastrzebski, Nicolas Ballas, David Krueger, Emmanuel Bengio, Maxinder S Kanwal, Tegan Maharaj, Asja Fischer, Aaron Courville, Yoshua Bengio, et al. A closer look at memorization in deep networks. In *International conference on machine learning*, pp. 233–242. PMLR, 2017.

Arthur Asuncion and David Newman. Uci machine learning repository, 2007.

Alexei Baevski, Yuhao Zhou, Abdelrahman Mohamed, and Michael Auli. wav2vec 2.0: A framework for self-supervised learning of speech representations. *Advances in neural information processing systems*, 33:12449–12460, 2020.

Dara Bahri, Heinrich Jiang, Yi Tay, and Donald Metzler. Scarf: Self-supervised contrastive learning using random feature corruption. *arXiv preprint arXiv:2106.15147*, 2021.

Gregory Benton, Marc Finzi, Pavel Izmailov, and Andrew G Wilson. Learning invariances in neural networks from training data. *Advances in neural information processing systems*, 33:17605–17616, 2020.

Davis Blalock, Jose Javier Gonzalez Ortiz, Jonathan Frankle, and John Guttag. What is the state of neural network pruning? *Proceedings of machine learning and systems*, 2:129–146, 2020.

Vadim Borisov, Tobias Leemann, Kathrin Seßler, Johannes Haug, Martin Pawelczyk, and Gjergji Kasneci. Deep neural networks and tabular data: A survey. *IEEE Transactions on Neural Networks and Learning Systems*, 2022.

Michael M Bronstein, Joan Bruna, Yann LeCun, Arthur Szlam, and Pierre Vandergheynst. Geometric deep learning: going beyond euclidean data. *IEEE Signal Processing Magazine*, 34(4):18–42, 2017.

Tianqi Chen and Carlos Guestrin. Xgboost: A scalable tree boosting system. In *Proceedings of the 22nd acm sigkdd international conference on knowledge discovery and data mining*, pp. 785–794, 2016.

Ting Chen, Simon Kornblith, Mohammad Norouzi, and Geoffrey Hinton. A simple framework for contrastive learning of visual representations. In *International conference on machine learning*, pp. 1597–1607. PMLR, 2020.

Xinlei Chen, Saining Xie, and Kaiming He. An empirical study of training self-supervised vision transformers. In *Proceedings of the IEEE/CVF International Conference on Computer Vision*, pp. 9640–9649, 2021.

Lenaic Chizat, Edouard Oyallon, and Francis Bach. On lazy training in differentiable programming. *Advances in neural information processing systems*, 32, 2019.

Sumit Chopra, Raia Hadsell, and Yann LeCun. Learning a similarity metric discriminatively, with application to face verification. In *2005 IEEE Computer Society Conference on Computer Vision and Pattern Recognition (CVPR'05)*, volume 1, pp. 539–546. IEEE, 2005.

Taco Cohen and Max Welling. Group equivariant convolutional networks. In *International conference on machine learning*, pp. 2990–2999. PMLR, 2016.

Francesco Corti, Rahim Entezari, Sara Hooker, Davide Bacciu, and Olga Saukh. Studying the impact of magnitude pruning on contrastive learning methods. *arXiv preprint arXiv:2207.00200*, 2022.

Ekin D Cubuk, Barret Zoph, Dandelion Mane, Vijay Vasudevan, and Quoc V Le. Autoaugment: Learning augmentation policies from data. *arXiv preprint arXiv:1805.09501*, 2018.

George Cybenko. Approximation by superpositions of a sigmoidal function. *Mathematics of control, signals and systems*, 2(4):303–314, 1989.

Rumen Dangovski, Li Jing, Charlotte Loh, Seungwook Han, Akash Srivastava, Brian Cheung, Pulkit Agrawal, and Marin Soljačić. Equivariant contrastive learning. *arXiv preprint arXiv:2111.00899*, 2021.

Michaël Defferrard, Xavier Bresson, and Pierre Vandergheynst. Convolutional neural networks on graphs with fast localized spectral filtering. *Advances in neural information processing systems*, 29, 2016.

Nima Dehmamy, Robin Walters, Yanchen Liu, Dashun Wang, and Rose Yu. Automatic symmetry discovery with lie algebra convolutional network. *Advances in Neural Information Processing Systems*, 34:2503–2515, 2021.

Valentin Delchevalerie, Adrien Bibal, Benoît Frénay, and Alexandre Mayer. Achieving rotational invariance with bessel-convolutional neural networks. *Advances in Neural Information Processing Systems*, 34:28772–28783, 2021.

Congyue Deng, Or Litany, Yueqi Duan, Adrien Poulenard, Andrea Tagliasacchi, and Leonidas J Guibas. Vector neurons: A general framework for so (3)-equivariant networks. In *Proceedings of the IEEE/CVF International Conference on Computer Vision*, pp. 12200–12209, 2021.

Utku Evci, Trevor Gale, Jacob Menick, Pablo Samuel Castro, and Erich Elsen. Rigging the lottery: Making all tickets winners. In *International Conference on Machine Learning*, pp. 2943–2952. PMLR, 2020.

Jonathan Frankle and Michael Carbin. The lottery ticket hypothesis: Finding sparse, trainable neural networks. *arXiv preprint arXiv:1803.03635*, 2018.

Pieter Gijsbers, Erin LeDell, Janek Thomas, Sébastien Poirier, Bernd Bischl, and Joaquin Vanschoren. An open source automl benchmark. *arXiv preprint arXiv:1907.00909*, 2019.

Xavier Glorot and Yoshua Bengio. Understanding the difficulty of training deep feedforward neural networks. In *Proceedings of the thirteenth international conference on artificial intelligence and statistics*, pp. 249–256. JMLR Workshop and Conference Proceedings, 2010.

Yury Gorishniy, Ivan Rubachev, Valentin Khrulkov, and Artem Babenko. Revisiting deep learning models for tabular data. *Advances in Neural Information Processing Systems*, 34:18932–18943, 2021.

Yury Gorishniy, Ivan Rubachev, and Artem Babenko. On embeddings for numerical features in tabular deep learning. *Advances in Neural Information Processing Systems*, 35:24991–25004, 2022.

Léo Grinsztajn, Edouard Oyallon, and Gaël Varoquaux. Why do tree-based models still outperform deep learning on tabular data? *arXiv preprint arXiv:2207.08815*, 2022.

Hussein Hazimeh, Natalia Ponomareva, Petros Mol, Zhenyu Tan, and Rahul Mazumder. The tree ensemble layer: Differentiability meets conditional computation. In *International Conference on Machine Learning*, pp. 4138–4148. PMLR, 2020.

Kaiming He, Xiangyu Zhang, Shaoqing Ren, and Jian Sun. Delving deep into rectifiers: Surpassing human-level performance on imagenet classification. In *Proceedings of the IEEE international conference on computer vision*, pp. 1026–1034, 2015.

Kaiming He, Xiangyu Zhang, Shaoqing Ren, and Jian Sun. Deep residual learning for image recognition. In *Proceedings of the IEEE conference on computer vision and pattern recognition*, pp. 770–778, 2016.

Duc NM Hoang, Shiwei Liu, Radu Marculescu, and Zhangyang Wang. Revisiting pruning at initialization through the lens of ramanujan graph. In *The Eleventh International Conference on Learning Representations*, 2023.

Noah Hollmann, Samuel Müller, Katharina Eggensperger, and Frank Hutter. Tabpfn: A transformer that solves small tabular classification problems in a second. *arXiv preprint arXiv:2207.01848*, 2022.

Sara Hooker, Aaron Courville, Gregory Clark, Yann Dauphin, and Andrea Frome. What do compressed deep neural networks forget? *arXiv preprint arXiv:1911.05248*, 2019.

Gao Huang, Yixuan Li, Geoff Pleiss, Zhuang Liu, John E Hopcroft, and Kilian Q Weinberger. Snapshot ensembles: Train 1, get m for free. *arXiv preprint arXiv:1704.00109*, 2017.

Xin Huang, Ashish Khetan, Milan Cvitkovic, and Zohar Karnin. Tabtransformer: Tabular data modeling using contextual embeddings. *arXiv preprint arXiv:2012.06678*, 2020.

Alexander Immer, Tycho van der Ouderaa, Gunnar Rätsch, Vincent Fortuin, and Mark van der Wilk. Invariance learning in deep neural networks with differentiable laplace approximations. *Advances in Neural Information Processing Systems*, 35:12449–12463, 2022.

Max Jaderberg, Karen Simonyan, Andrew Zisserman, et al. Spatial transformer networks. *Advances in neural information processing systems*, 28, 2015.

Ashish Jaiswal, Ashwin Ramesh Babu, Mohammad Zaki Zadeh, Debapriya Banerjee, and Fillia Makedon. A survey on contrastive self-supervised learning. *Technologies*, 9(1):2, 2020.

Manu Joseph and Harsh Raj. Gate: Gated additive tree ensemble for tabular classification and regression. *arXiv preprint arXiv:2207.08548*, 2022.

Arlind Kadra, Marius Lindauer, Frank Hutter, and Josif Grabocka. Well-tuned simple nets excel on tabular datasets. *Advances in neural information processing systems*, 34:23928–23941, 2021.

Liran Katzir, Gal Elidan, and Ran El-Yaniv. Net-dnf: Effective deep modeling of tabular data. In *International conference on learning representations*, 2020.

Thomas N Kipf and Max Welling. Semi-supervised classification with graph convolutional networks. *arXiv preprint arXiv:1609.02907*, 2016.

Louis Kirsch, Sebastian Flennerhag, Hado van Hasselt, Abram Friesen, Junhyuk Oh, and Yutian Chen. Introducing symmetries to black box meta reinforcement learning. In *Proceedings of the AAAI Conference on Artificial Intelligence*, volume 36, pp. 7202–7210, 2022.

Alex Krizhevsky, Geoffrey Hinton, et al. Learning multiple layers of features from tiny images. 2009.

Yann LeCun, Léon Bottou, Yoshua Bengio, and Patrick Haffner. Gradient-based learning applied to document recognition. *Proceedings of the IEEE*, 86(11):2278–2324, 1998.

Yann LeCun, Yoshua Bengio, and Geoffrey Hinton. Deep learning. *nature*, 521(7553):436–444, 2015.

Namhoon Lee, Thalaiyasingam Ajanthan, Stephen Gould, and Philip HS Torr. A signal propagation perspective for pruning neural networks at initialization. *arXiv preprint arXiv:1906.06307*, 2019.

Hanxiao Liu, Karen Simonyan, and Yiming Yang. Darts: Differentiable architecture search. *arXiv preprint arXiv:1806.09055*, 2018a.

Shiwei Liu, Tianlong Chen, Zhenyu Zhang, Xuxi Chen, Tianjin Huang, Ajay Jaiswal, and Zhangyang Wang. Sparsity may cry: Let us fail (current) sparse neural networks together! *arXiv preprint arXiv:2303.02141*, 2023.

Zhuang Liu, Mingjie Sun, Tinghui Zhou, Gao Huang, and Trevor Darrell. Rethinking the value of network pruning. *arXiv preprint arXiv:1810.05270*, 2018b.

Jonathan Lorraine, Paul Vicol, and David Duvenaud. Optimizing millions of hyperparameters by implicit differentiation. In *International Conference on Artificial Intelligence and Statistics*, pp. 1540–1552. PMLR, 2020.

Ilya Loshchilov and Frank Hutter. Decoupled weight decay regularization. *arXiv preprint arXiv:1711.05101*, 2017.

Christos Louizos, Max Welling, and Diederik P Kingma. Learning sparse neural networks through l_0 regularization. *arXiv preprint arXiv:1712.01312*, 2017.

Renqian Luo, Fei Tian, Tao Qin, Enhong Chen, and Tie-Yan Liu. Neural architecture optimization. *Advances in neural information processing systems*, 31, 2018.

Xiaolong Ma, Geng Yuan, Xuan Shen, Tianlong Chen, Xuxi Chen, Xiaohan Chen, Ning Liu, Minghai Qin, Sijia Liu, Zhangyang Wang, et al. Sanity checks for lottery tickets: Does your winning ticket really win the jackpot? *Advances in Neural Information Processing Systems*, 34:12749–12760, 2021.

Yuval Netzer, Tao Wang, Adam Coates, Alessandro Bissacco, Bo Wu, and Andrew Y Ng. Reading digits in natural images with unsupervised feature learning. 2011.

Behnam Neyshabur. Implicit regularization in deep learning. *arXiv preprint arXiv:1709.01953*, 2017.

Behnam Neyshabur. Towards learning convolutions from scratch. *Advances in Neural Information Processing Systems*, 33:8078–8088, 2020.

Behnam Neyshabur, Ryota Tomioka, and Nathan Srebro. In search of the real inductive bias: On the role of implicit regularization in deep learning. *arXiv preprint arXiv:1412.6614*, 2014.

Hyun Oh Song, Yu Xiang, Stefanie Jegelka, and Silvio Savarese. Deep metric learning via lifted structured feature embedding. In *Proceedings of the IEEE conference on computer vision and pattern recognition*, pp. 4004–4012, 2016.

Ankita Pasad, Ju-Chieh Chou, and Karen Livescu. Layer-wise analysis of a self-supervised speech representation model. In *2021 IEEE Automatic Speech Recognition and Understanding Workshop (ASRU)*, pp. 914–921. IEEE, 2021.

Hieu Pham, Melody Guan, Barret Zoph, Quoc Le, and Jeff Dean. Efficient neural architecture search via parameters sharing. In *International conference on machine learning*, pp. 4095–4104. PMLR, 2018.

Sergei Popov, Stanislav Morozov, and Artem Babenko. Neural oblivious decision ensembles for deep learning on tabular data. *arXiv preprint arXiv:1909.06312*, 2019.

Charles Ruizhongtai Qi, Li Yi, Hao Su, and Leonidas J Guibas. Pointnet++: Deep hierarchical feature learning on point sets in a metric space. *Advances in neural information processing systems*, 30, 2017.

Facundo Quiroga, Franco Ronchetti, Laura Lanzarini, and Aurelio F Bariviera. Revisiting data augmentation for rotational invariance in convolutional neural networks. In *Modelling and Simulation in Management Sciences: Proceedings of the International Conference on Modelling and Simulation in Management Sciences (MS-18)*, pp. 127–141. Springer, 2020.

Sara Sabour, Nicholas Frosst, and Geoffrey E Hinton. Dynamic routing between capsules. *Advances in neural information processing systems*, 30, 2017.

Vıctor Garcia Satorras, Emiel Hoogeboom, and Max Welling. E (n) equivariant graph neural networks. In *International conference on machine learning*, pp. 9323–9332. PMLR, 2021.

Bernhard Schäfl, Lukas Gruber, Angela Bitto-Nemling, and Sepp Hochreiter. Hopular: Modern hopfield networks for tabular data. *arXiv preprint arXiv:2206.00664*, 2022.

Florian Schroff, Dmitry Kalenichenko, and James Philbin. Facenet: A unified embedding for face recognition and clustering. In *Proceedings of the IEEE conference on computer vision and pattern recognition*, pp. 815–823, 2015.

Ravid Shwartz-Ziv and Amitai Armon. Tabular data: Deep learning is not all you need. *Information Fusion*, 81:84–90, 2022.

Vasu Singla, Songwei Ge, Basri Ronen, and David Jacobs. Shift invariance can reduce adversarial robustness. *Advances in Neural Information Processing Systems*, 34:1858–1871, 2021.

Gowthami Somepalli, Micah Goldblum, Avi Schwarzschild, C Bayan Bruss, and Tom Goldstein. Saint: Improved neural networks for tabular data via row attention and contrastive pre-training. *arXiv preprint arXiv:2106.01342*, 2021.

Ilya O Tolstikhin, Neil Houlsby, Alexander Kolesnikov, Lucas Beyer, Xiaohua Zhai, Thomas Unterthiner, Jessica Yung, Andreas Steiner, Daniel Keysers, Jakob Uszkoreit, et al. Mlp-mixer: An all-mlp architecture for vision. *Advances in neural information processing systems*, 34:24261–24272, 2021.

Belinda Tzen and Maxim Raginsky. A mean-field theory of lazy training in two-layer neural nets: entropic regularization and controlled mckean-vlasov dynamics. *arXiv preprint arXiv:2002.01987*, 2020.

Ashish Vaswani, Noam Shazeer, Niki Parmar, Jakob Uszkoreit, Llion Jones, Aidan N Gomez, Łukasz Kaiser, and Illia Polosukhin. Attention is all you need. *Advances in neural information processing systems*, 30, 2017.

Alvin Wan, Xiaoliang Dai, Peizhao Zhang, Zijian He, Yuandong Tian, Saining Xie, Bichen Wu, Matthew Yu, Tao Xu, Kan Chen, et al. Fbnetv2: Differentiable neural architecture search for spatial and channel dimensions. In *Proceedings of the IEEE/CVF Conference on Computer Vision and Pattern Recognition*, pp. 12965–12974, 2020.

Chaoqi Wang, Guodong Zhang, and Roger Grosse. Picking winning tickets before training by preserving gradient flow. *arXiv preprint arXiv:2002.07376*, 2020.

Zonghan Wu, Shirui Pan, Fengwen Chen, Guodong Long, Chengqi Zhang, and S Yu Philip. A comprehensive survey on graph neural networks. *IEEE transactions on neural networks and learning systems*, 32(1):4–24, 2020.

Saining Xie, Alexander Kirillov, Ross Girshick, and Kaiming He. Exploring randomly wired neural networks for image recognition. In *Proceedings of the IEEE/CVF International Conference on Computer Vision*, pp. 1284–1293, 2019.

Yichong Xu, Tianjun Xiao, Jiaxing Zhang, Kuiyuan Yang, and Zheng Zhang. Scale-invariant convolutional neural networks. *arXiv preprint arXiv:1411.6369*, 2014.

Jiaxuan You, Jure Leskovec, Kaiming He, and Saining Xie. Graph structure of neural networks. In *International Conference on Machine Learning*, pp. 10881–10891. PMLR, 2020a.

Yuning You, Tianlong Chen, Yongduo Sui, Ting Chen, Zhangyang Wang, and Yang Shen. Graph contrastive learning with augmentations. *Advances in neural information processing systems*, 33: 5812–5823, 2020b.

Chiyuan Zhang, Samy Bengio, Moritz Hardt, Benjamin Recht, and Oriol Vinyals. Understanding deep learning (still) requires rethinking generalization. *Communications of the ACM*, 64(3):107–115, 2021.

Tianyi Zhang, Felix Wu, Arzoo Katiyar, Kilian Q Weinberger, and Yoav Artzi. Revisiting few-sample bert fine-tuning. *arXiv preprint arXiv:2006.05987*, 2020.

Allan Zhou, Tom Knowles, and Chelsea Finn. Meta-learning symmetries by reparameterization. *arXiv preprint arXiv:2007.02933*, 2020.

Yanqiao Zhu, Yichen Xu, Feng Yu, Qiang Liu, Shu Wu, and Liang Wang. Graph contrastive learning with adaptive augmentation. In *Proceedings of the Web Conference 2021*, pp. 2069–2080, 2021.

Lucas Zimmer, Marius Lindauer, and Frank Hutter. Auto-pytorch: Multi-fidelity metalearning for efficient and robust autodl. *IEEE Transactions on Pattern Analysis and Machine Intelligence*, 43 (9):3079–3090, 2021.

Barret Zoph, Vijay Vasudevan, Jonathon Shlens, and Quoc V Le. Learning transferable architectures for scalable image recognition. In *Proceedings of the IEEE conference on computer vision and pattern recognition*, pp. 8697–8710, 2018.

A Additional Related Work

A.1 Tabular Machine Learning

Tabular data is a difficult regime for deep learning, where deep learning models struggle against decision tree approaches. Early methods use forests, ensembling, and boosting (Shwartz-Ziv & Armon, 2022; Borisov et al., 2022; Chen & Guestrin, 2016). Later, researchers handcrafted new deep architectures that mimic trees (Popov et al., 2019; Katzir et al., 2020; Huang et al., 2020; Hazimeh et al., 2020; Somepalli et al., 2021; Arik & Pfister, 2021). Yet, when evaluated on large datasets, these approaches are still beaten by XGB (Chen & Guestrin, 2016; Grinsztajn et al., 2022). Recent work found MLPs with heavy regularization tuning (Kadra et al., 2021) can outperform decision tree approaches, though this conclusion does not hold on small tabular datasets (Joseph & Raj, 2022). To specially tackle the small data regime, Bayesian learning and Hopfield networks are combined with MLPs (Hollmann et al., 2022; Schäfl et al., 2022). There are also work on tabular transformers (Huang et al., 2020; Gorishniy et al., 2021), though said approaches require much more training data. Without regularization, tree based models still outperform MLPs due to a better inductive bias and resilience to noise (Grinsztajn et al., 2022). Different data preprocessing level encodings are being proposed to boost MLP performance (Gorishniy et al., 2022). To the best of our knowledge, the state-of-the-art on general tabular datasets remain heavily regularized MLPs ($\text{MLP}_{\text{TAB+C}}$) (Kadra et al., 2021; Gorishniy et al., 2022). We aim to further boost regularized MLP performance by discovering model architectures that capture good invariances from tabular data.

A.2 Contrastive Learning

Contrastive learning, initially proposed for metric learning (Chopra et al., 2005; Schroff et al., 2015; Oh Song et al., 2016), trains a model to learn shared features among images of the same type (Jaiswal et al., 2020). It has been widely used in self-supervised pretraining (Chen et al., 2020; 2021), where dataset augmentation is crucial. Although contrastive learning was originally proposed for images, it has also shown promising results in graph data (Zhu et al., 2021; You et al., 2020b), speech data (Baevski et al., 2020), and tabular data (Bahri et al., 2021). Previous study has showed that speech transformers tend to overfit the contrastive loss in deeper layers, suggesting that removing later layers can be beneficial during finetuning (Pasad et al., 2021). While contrastive learning performs well pretraining unpruned models, its vanilla formulation performs poorly after network pruning (Corti et al., 2022). In this work, we establish a connection between contrastive learning and invariance learning and observe that pruned contrastive models fail because of overfitting.

A.3 Neural Architecture Search

Neural Architecture Search (NAS) explores large superarchitectures by leveraging smaller block architectures (Wan et al., 2020; Pham et al., 2018; Zoph et al., 2018; Luo et al., 2018; Liu et al., 2018a). These block architectures are typically small convolutional neural networks (CNNs) or MLPs. The key idea behind NAS is to utilize these blocks (Pham et al., 2018; Zoph et al., 2018) to capture desired invariance properties for downstream tasks. Prior works (You et al., 2020a; Xie et al., 2019) have analyzed randomly selected intra- and inter-block structures and observed performance differences between said structures. However, these work did not propose a method for discovering block architectures directly from data. Our work aims to address this gap by focusing on discovering the architecture within NAS blocks. This approach has the potential to enable NAS in diverse domains, expanding its applicability beyond the current scope.

B Loss Function Details

We provide a more detailed description of our loss function in this section. Following notation from the main paper, we repeat the ILO loss function in Equation 7 below:

$$\mathcal{L}(\theta; \mathcal{S}) = \mathbb{E}_{x,y \sim D_{train}} \left[\mathcal{L}_{SUP}(x, y, \theta) + \lambda \mathcal{L}_{NCE}(x, y, \theta; \mathcal{S}) \right] \tag{7}$$

To better explain our loss functions, we introduce some new notations. First, we denote the decoder output probability function over classes, $\mathcal{Y}$, as $\tilde{p}_{\theta_\mathcal{D}} : \mathcal{H} \rightarrow [0, 1]^{|\mathcal{Y}|}$, where $f_\mathcal{D} = \text{argmax} \circ \tilde{p}_{\theta_\mathcal{D}}$. We denote the model output probability function by combining $\tilde{p}_{\theta_\mathcal{D}}$ with the encoder as follows: $p_\theta = \tilde{p}_{\theta_\mathcal{D}} \circ f_\mathcal{E}$. We introduce an integer mapping from classes $\mathcal{Y}$ as $\mathcal{I} : \mathcal{Y} \rightarrow \{0, 1, 2, ..., |\mathcal{Y}| - 1\}$.

We show the maximum likelihood loss, $\mathcal{L}_{SUP}$, in Equation 8 below.

$$\mathcal{L}_{SUP}(x, y, \theta) = -log(p_\theta(x, \theta)_{\mathcal{I}(y)}) \tag{8}$$

We show the supervised contrastive loss, $\mathcal{L}_{NCE}$, in Equation 9 below. Following SimCLR (Chen et al., 2020), we assume that the intermediary representations are d-dimensional embeddings, $\mathcal{H} = \mathbb{R}^d$, and use the cosine similarity as our similarity function, $\psi^{(cos)} : \mathbb{R}^d \times \mathbb{R}^d \rightarrow \mathbb{R}$.

$$\mathcal{L}_{NCE}(x, y, \theta; \mathcal{S}) = \mathop{\mathbb{E}}_{g \sim \mathcal{S}} \left[-log \left(\frac{exp\left(\psi^{(cos)}\left(f_\mathcal{E}(x; \theta), f_\mathcal{E}(g(x); \theta)\right)\right)}{\sum\limits_{\substack{x', y' \sim D_{tr} \\ y' \neq y}} exp\left(\psi^{(cos)}\left(f_\mathcal{E}(x; \theta), f_\mathcal{E}(g(x'); \theta)\right)\right)} \right) \right] \tag{9}$$

B.1 Surrogate Objective

We aim to learn invariance-preserving network architectures from the data. In our framework, this involves optimizing our invariance objective, which we repeat in Equation 10. We prove Theorem 1, that minimizing the supervised contrastive loss is equivalent to maximizing the invariance objective, outlined below.

$$\theta^* = \underset{\theta}{argmax} \mathop{\mathbb{E}}_{\substack{x_i, x_j \sim \mathcal{X} \\ g \sim \mathcal{S}}} \left[\frac{\phi(f_\mathcal{E}^M(x_i; \theta), f_\mathcal{E}^M(x_j; \theta))}{\phi(f_\mathcal{E}^M(x_i; \theta), f_\mathcal{E}^M(g(x_i); \theta))} \right] \tag{10}$$

We convert the distance metric ϕ into similarity metric ψ.

Dataset	$g(\cdot)$	MLP$_{\text{VIS}}$	IUNET $^{(\text{MLP}_{\text{VIS}})}$
CIFAR10	resize.	44.096 ± 0.434	**97.349** $\pm$ **4.590**
	horiz.	80.485 ± 0.504	**99.413** $\pm$ **1.016**
	color.	56.075 ± 0.433	**98.233** $\pm$ **3.060**
	graysc.	81.932 ± 0.233	**99.077** $\pm$ **1.598**
CIFAR100	resize.	32.990 ± 1.065	**39.936** $\pm$ **2.786**
	horiz.	70.793 ± 0.677	**77.935** $\pm$ **1.464**
	color.	31.704 ± 0.560	**51.397** $\pm$ **2.709**
	graysc.	71.245 ± 0.467	**76.476** $\pm$ **1.245**
SVHN	resize.	36.708 ± 2.033	**77.440** $\pm$ **0.627**
	horiz.	71.400 ± 1.651	**95.082** $\pm$ **0.166**
	color.	61.341 ± 0.946	**91.097** $\pm$ **0.395**
	graysc.	90.344 ± 0.233	**99.259** $\pm$ **0.073**

Table 5: Comparing the consistency metric (%) of the untrained supernetwork, MLP$_{\text{VIS}}$ and MLP$_{\text{TAB}}$, against IUNET's pruned subnetwork under different invariant transforms, $g(\cdot)$. IUNET preserves invariances better.

$$
\begin{aligned}
\theta^* &= \underset{\theta}{argmax} \underset{\substack{x_i, x_j \sim \mathcal{X} \\ g \sim \mathcal{S}}}{\mathbb{E}} \left[\frac{\psi(f_{\mathcal{E}}^M(x_i;\theta), f_{\mathcal{E}}^M(g(x_i);\theta))}{\psi(f_{\mathcal{E}}^M(x_i;\theta), f_{\mathcal{E}}^M(x_j;\theta))} \right] \\
&= \underset{\theta}{argmin} \underset{\substack{x_i, x_j \sim \mathcal{X} \\ g \sim \mathcal{S}}}{\mathbb{E}} \left[\frac{-\psi(f_{\mathcal{E}}^M(x_i;\theta), f_{\mathcal{E}}^M(g(x_i);\theta))}{\psi(f_{\mathcal{E}}^M(x_i;\theta), f_{\mathcal{E}}^M(x_j;\theta))} \right] \\
&= \underset{\theta}{argmin} \underset{\substack{x \sim \mathcal{X} \\ g \sim \mathcal{S}}}{\mathbb{E}} \left[\frac{-\psi(f_{\mathcal{E}}^M(x;\theta), f_{\mathcal{E}}^M(g(x);\theta))}{\sum\limits_{\substack{x' \sim \mathcal{X} \\ x' \neq x}} \psi(f_{\mathcal{E}}^M(x;\theta), f_{\mathcal{E}}^M(g(x');\theta))} \right] \\
&= \underset{\theta}{argmin} \underset{\substack{x, y \sim D_{tr} \\ g \sim \mathcal{S}}}{\mathbb{E}} \left[\frac{-\psi\left(f_{\mathcal{E}}^M(x;\theta), f_{\mathcal{E}}^M(g(x);\theta)\right)}{\sum\limits_{\substack{x', y' \sim D_{tr} \\ y' \neq y}} \psi\left(f_{\mathcal{E}}^M(x;\theta), f_{\mathcal{E}}^M(g(x');\theta)\right)} \right] \\
&= \underset{\theta}{argmin} \underset{\substack{x, y \sim D_{tr} \\ g \sim \mathcal{S}}}{\mathbb{E}} \left[-log \left(\frac{\psi\left(f_{\mathcal{E}}^M(x;\theta), f_{\mathcal{E}}^M(g(x);\theta)\right)}{\sum\limits_{\substack{x', y' \sim D_{tr} \\ y' \neq y}} \psi\left(f_{\mathcal{E}}^M(x;\theta), f_{\mathcal{E}}^M(g(x');\theta)\right)} \right) \right]
\end{aligned} \tag{11}
$$

We set the similarity metric, ψ, to be the same as our contrastive loss: $\psi(\cdot) = exp(\psi^{(cos)}(\cdot))$.

$$
\theta^* = \underset{\theta}{argmin} \underset{x, y \sim D_{train}}{\mathbb{E}} [\mathcal{L}_{NCE}(x, y, \theta; \mathcal{S})] \tag{12}
$$

Here, we showed that the vanilla contrastive loss function, Equation 9, serves as a surrogate objective for optimizing our desired invariance objective, Equation 10. By incorporating contrastive learning alongside the maximum likelihood objective in Equation 7, ILO effectively reveals the underlying invariances in the pruned model.

C Additional Discussion on Lazy Training

The lazy training regime (Chizat et al., 2019; Tzen & Raginsky, 2020) is a phenomenon when loss rapidly decreases, while weight values stay relatively constant. This phenomenon occurs on large

Dataset	MLP_{VIS}	IUNET $^{(\text{MLP}_{\text{VIS}})}$	CNN	IUNET $^{(\text{RESNET})}$
CIFAR10	59.266 ± 0.050	64.847 ± 0.121	75.850 ± 0.788	$\mathbf{83.729 \pm 0.153}$
CIFAR100	31.052 ± 0.371	32.760 ± 0.288	41.634 ± 0.402	$\mathbf{53.099 \pm 0.243}$
SVHN	84.463 ± 0.393	89.357 ± 0.156	91.892 ± 0.411	$\mathbf{94.020 \pm 0.291}$

Table 6: Comparing the pruned IUNET $^{(\text{MLP}_{\text{VIS}})}$ model to a CNN which is architecturally equivalent to IUNET $^{(\text{MLP}_{\text{VIS}})}$ in terms of layer count and hidden dimensions with the only differences being network structure and weight sharing. Although IUNET $^{(\text{MLP}_{\text{VIS}})}$ cannot outperform CNN, it bridges the gap between MLP and CNN architectures without any human design intervention.

over-parameterized neural networks (Chizat et al., 2019). Because the weight values stay relatively constant, the magnitude ordering between weights also changes very little. Therefore, network pruning struggles to preserve such loss decreases in the lazy training regime (Liu et al., 2023).

Because weights with very small magnitude have minimal effect on the output logits, pruning said weights will not drastically hurt performance. Thus, if the pruning framework can separate very small magnitude weights from normal weights prior to the lazy training regime, we can preserve loss decreases in the lazy training regime. The PIS setting accomplishes this by initializing all weights to be very small so that only important weights will learn large magnitudes. This guarantees that a large percentage of weights will have small magnitudes throughout training, while important larger magnitude weights will emerge over the course of training.

D ADDITIONAL EXPERIMENTS

D.1 ON TABULAR DATASETS: FULL RESULTS

We provide the full tabular dataset results in Table 7. As shown, the trends reported in the main text holds on the whole dataset.

D.2 ON CONSISTENCY: FULL RESULTS

We provide consistency experiments on CIFAR100 and SVHN in Table 5. As shown, the trends reported in the main text holds on other datasets.

D.3 COMPARING IUNET WITH CNN

We compare IUNET $^{(\text{MLP}_{\text{VIS}})}$ with a CNN in Table 6. Unlike IUNET $^{(\text{MLP}_{\text{VIS}})}$, CNNs also employ weight sharing. While IUNET consistently improves performance of both MLP_{VIS} and RESNET via pruning the model architecture, exploration of weight sharing is an orthogonal direction that could also reduce the gap between MLPs and CNNs. Note, IUNET $^{(\text{RESNET})}$ still performs the best out of all models.

E IMPLEMENTATION DETAILS

E.1 DATASET DETAILS

We considered the following *computer vision* datasets: CIFAR10, CIFAR100 (Krizhevsky et al., 2009), and SVHN (Netzer et al., 2011). CIFAR10 and CIFAR100 are multi-domain image classification datasets. SVHN is a street sign digit classification dataset. Input images are 32×32 color images. We split the train set by 80/20 for training and validation. We test on the test set provided separately. We reported dataset statistics in Table 8.

We considered 40 tabular datasets from OpenML (Gijsbers et al., 2019), UCI (Asuncion & Newman, 2007), and Kaggle, following the $\text{MLP}_{\text{TAB+C}}$ benchmark (Kadra et al., 2021). These tabular datasets cover a variety of domains, data types, and class imbalances. We used a 60/20/20 train validation test split, and reported dataset statistics in Table 9. We use a random seed of 11 for the data split, following prior work (Kadra et al., 2021).

Dataset	MLP_{TAB}	OMP	β-LASSO	IUNET	XGB	TABN	$\text{MLP}_{\text{TAB+C}}$
credit-g	70.000	70.000	67.205	63.166 ± 0.000	68.929	61.190	**74.643**
anneal	99.490	99.691	99.634	**99.712 ± 0.101**	85.416	84.248	89.270
kr-vs-kp	99.158	99.062	99.049	99.151 ± 0.064	**99.850**	93.250	**99.850**
arrhythmia	67.086	55.483	67.719	**74.138 ± 2.769**	48.779	43.562	61.461
mfeat.	98.169	97.959	97.204	**98.176 ± 0.121**	98.000	97.250	98.000
vehicle	80.427	81.115	80.611	81.805 ± 2.065	74.973	79.654	**82.576**
kc1	80.762	**84.597**	83.587	**84.597 ± 0.000**	66.846	52.517	74.381
adult	81.968	82.212	82.323	78.249 ± 3.085	79.824	77.155	**82.443**
walking.	58.466	60.033	58.049	59.789 ± 0.456	61.616	56.801	**63.923**
phoneme	84.213	86.733	84.850	87.284 ± 0.436	**87.972**	86.824	86.619
skin-seg.	99.869	99.866	99.851	99.876 ± 0.006	**99.968**	99.961	99.953
ldpa	66.590	68.458	62.362	64.816 ± 4.535	**99.008**	54.815	68.107
nomao	95.776	95.682	95.756	95.703 ± 0.110	**96.872**	95.425	96.826
cnae	94.080	92.742	94.808	**96.075 ± 0.242**	94.907	89.352	95.833
blood.	68.965	61.841	65.126	**70.375 ± 5.255**	62.281	64.327	67.617
bank.	**88.300**	**88.300**	86.923	**88.300 ± 0.000**	72.658	70.639	85.993
connect.	72.111	72.016	72.400	74.475 ± 0.445	72.374	72.045	**80.073**
shuttle	99.709	93.791	99.687	93.735 ± 2.303	98.563	88.017	**99.948**
higgs	72.192	72.668	72.263	73.215 ± 0.384	72.944	72.036	**73.546**
australian	82.153	83.942	81.667	82.562 ± 1.927	**89.717**	85.278	87.088
car	99.966	**100.000**	**100.000**	99.859 ± 0.200	92.376	98.701	99.587
segment	91.504	91.603	91.317	91.563 ± 0.000	**93.723**	91.775	**93.723**
fashion.	91.139	90.784	90.864	90.817 ± 0.040	91.243	89.793	**91.950**
jungle.	86.998	92.071	87.400	95.130 ± 0.807	87.325	73.425	**97.471**
numerai	51.621	51.443	51.905	51.839 ± 0.067	52.363	51.599	**52.668**
devnagari	97.550	97.573	97.549	97.517 ± 0.014	93.310	94.179	**98.370**
helena	29.342	28.459	29.834	**29.884 ± 0.991**	21.994	19.032	27.701
jannis	68.647	66.302	69.302	**69.998 ± 1.232**	55.225	56.214	65.287
volkert	70.066	68.781	69.655	70.104 ± 0.215	64.170	59.409	**71.667**
miniboone	86.539	87.575	87.751	81.226 ± 6.569	**94.024**	62.173	94.015
apsfailure	97.041	**98.191**	98.048	**98.191 ± 0.000**	88.825	51.444	92.535
christine	70.295	69.819	70.275	69.065 ± 1.225	**74.815**	69.649	74.262
dilbert	98.494	98.738	98.522	98.540 ± 0.023	**99.106**	97.608	99.049
fabert	65.540	64.709	66.681	65.695 ± 0.065	**70.098**	62.277	69.183
jasmine	78.691	80.139	78.415	**80.864 ± 0.374**	80.546	76.690	79.217
sylvine	92.660	92.650	92.593	93.369 ± 0.833	**95.509**	83.595	94.045
dionis	93.920	93.687	93.943	93.586 ± 0.021	91.222	83.960	**94.010**
aloi	96.546	96.376	96.562	95.341 ± 0.194	95.338	93.589	**97.175**
ccfraud	97.554	97.748	96.626	**98.797 ± 1.031**	90.303	85.705	92.531
clickpred.	82.175	83.206	82.307	**85.270 ± 1.275**	58.361	50.163	64.280

Table 7: Comparing IUNET against trees (XGB), handcrafted models (TABN), and state-of-the-art regularized MLPs ($\text{MLP}_{\text{TAB+C}}$). OMP, β-LASSO, and IUNET all modify MLP_{TAB}. Note, our method does not tune the optimal regularization settings for each dataset making it more efficient. Our pruned model is also more compressed than the original network. Note, we outperform both MLP_{TAB} and TABN on most datasets. While IUNET performs similarly to $\text{MLP}_{\text{TAB+C}}$, it does not require costly hyperparameter tuning, and can be applied on top of the optimal settings found by $\text{MLP}_{\text{TAB+C}}$.

E.2 HYPERPARAMETER SETTINGS

All experiments were run 3 times from scratch starting with different random seeds. We report both the mean and standard deviation of all runs. All hyperparameters were chosen based on validation set results.

For all experiments, we used $\lambda = 1$, which was chosen through a grid search over $\lambda \in \{0.25, 0.5, 1.0\}$. For all experiments, we used a batch size of 128. For pre-pruning training, we used SGD with Nesterov momentum and a learning rate of 0.001, following past works (Blalock et al., 2020). For finetuning vision datasets, we used the same optimizer setup except with 16-bit operations except for batch normalization, following β-LASSO (Neyshabur, 2020). For finetuning tabular datasets, we used AdamW (Loshchilov & Hutter, 2017), a learning rate of 0.001s, decoupled weight decay, cosine annealing with restart, initial restart budget of 15 epochs, budget multiplier of 2, and snapshot ensembling (Huang et al., 2017), following prior works (Kadra et al., 2021; Zimmer et al., 2021). It is important to note we did not tune the dataset and training hyperparameters for each tabular dataset individually like $\text{MLP}_{\text{TAB+C}}$ (Kadra et al., 2021), rather taking the most effective setting on average.

For tabular datasets, we tuned the compression ratio over the following range of values: $r \in \{2, 4, 8\}$ and the PIs multiplier over the following range of values: $\kappa \in \{0.25, 0.125, 0.0625\}$. on a subset of 4 tabular datasets. We found that $r = 8$ and $\kappa = 0.25$ performs the most consistently and used this setting for all runs of IUNET in the main paper. It is important to note we did not tune hyperparameters for IUNET on each individual tabular dataset like $\text{MLP}_{\text{TAB+C}}$ (Kadra et al., 2021), making IUNET a much more efficient model than $\text{MLP}_{\text{TAB+C}}$. For the tabular baselines (Chen & Guestrin, 2016; Arik & Pfister, 2021; Kadra et al., 2021), we used the same hyperparameter tuning setup as the MLP+C benchmark (Kadra et al., 2021).

For vision datasets, we tuned the compression ratio over the following range of values: $r \in \{2, 4, 8, 16\}$ on each individual dataset for all network pruning models except β-LASSO[5]. For β-lasso (Neyshabur, 2020), we tuned the hyperparameters over the range $\beta = \{50\}$ and L1 regularization in $l1 \in \{10^{-6}, 2 \times 10^{-6}, 5 \times 10^{-6}, 10^{-5}, 2 \times 10^{-5}\}$ on each individual dataset as done in the original paper. It is important to note that although we tuned both hyperparameters for both IUNET and baselines on each individual datasets, our main and ablation table rankings stay consistent had we chosen a single setting for all datasets, as shown in the detailed pruning experiments in the main paper.

E.3 SUPERNETWORK ARCHITECTURE

MLP_{VIS} is a deep MLP that contains a CNN subnetwork. Given a scaling factor, α, the CNN architecture consists of 3x3 convolutional layers with the following (out channels, stride) settings: $[(\alpha, 1)$, $(2\alpha, 2)$, $(2\alpha, 1)$, $(4\alpha, 2)$, $(4\alpha, 1)$, $(8\alpha, 2)$, $(8\alpha, 1)$, $(16\alpha, 2)]$ followed by a hidden layer of dimension 64α. It is worth noting that our CNN does not include maxpooling layers for fair comparison with the learned architectures, following the same setup as β-LASSO (Neyshabur, 2020). To form the MLP Network, we ensured the CNN network structure exists as a subnetwork within the MLP supernetwork by setting the hidden layer sizes to: $[\alpha s^2, \frac{\alpha s^2}{2}, \frac{\alpha s^2}{2}, \frac{\alpha s^2}{4}, \frac{\alpha s^2}{4}, \frac{\alpha s^2}{8}, \frac{\alpha s^2}{8}, \frac{\alpha s^2}{16}, 64\alpha]$. This architecture was also introduced in β-Lasso (Neyshabur, 2020). All layers are preceded by batch normalization and ReLU activation. We chose $\alpha = 8$ such that our supernetwork can fit onto an Nvidia RTX 3070 GPU.

CNN is the corresponding CNN subnetwork with (out channels, stride) settings: $[(\alpha, 1)$, $(2\alpha, 2)$, $(2\alpha, 1)$, $(4\alpha, 2)$, $(4\alpha, 1)$, $(8\alpha, 2)$, $(8\alpha, 1)$, $(16\alpha, 2)]$, derived from prior works (Neyshabur, 2020). Again, we chose $\alpha = 8$ to be consistent with MLP_{VIS}.

RESNET (He et al., 2016) is the standard RESNET-18 model used in past benchmarks (Blalock et al., 2020). Resnet differs from CNN in its inclusion of max-pooling layers and residual connections.

MLP_{TAB} is a 9-layer MLP with hidden dimension 512, batch normalization, and ReLU activation. We did not use dropout or skip connections as it was found to be ineffective on most tabular datasets in MLP+C (Kadra et al., 2021).

[5]This is because β-LASSO does not accept a chosen compression ratio as a hyperparameter.

Dataset	# Train Instances	# Valid Instances	# Test Instances	Number of Classes
CIFAR10	40000	10000	10000	10
CIFAR100	40000	10000	10000	100
SVHN	58606	14651	26032	10

Table 8: Statistics on computer vision datasets.

E.4 PRUNING IMPLEMENTATION DETAILS

Following Shrinkbench (Blalock et al., 2020), we use magnitude-based pruning only on the encoder, $f_{\mathcal{E}}$, keeping all weights in the decoder, $f_{\mathcal{D}}$. This is done to prevent pruning a cutset in the decoder architecture, so that all class logits receive input signal. To optimize the performance, we apply magnitude-based pruning globally, instead of layer-wise.

E.5 HARDWARE

All experiments were conducted on an Nvidia V100 GPU and an AMD EPYC 7402 CPU. The duration of the tabular experiments varied, ranging from a few minutes up to half a day, depending on the specific dataset-model pair and the training phase (pre-pruning training or finetuning). For the vision experiments, a single setting on a single dataset-model pair required a few hours for both pre-pruning training and finetuning.

Dataset	# Train Inst.	# Valid Inst.	# Test Inst.	# Feats.	Majority Class %	Minority Class %	OpenML ID
Anneal	538	179	179	39	76.17	0.89	233090
Kr-vs-kp	1917	639	639	37	52.22	47.78	233091
Arrhythmia	271	90	90	280	54.20	0.44	233092
Mfeat-factors	1200	400	400	217	10.00	10.00	233093
Credit-g	600	200	200	21	70.00	30.00	233088
Vehicle	507	169	169	19	25.77	23.52	233094
Kc1	1265	421	421	22	84.54	15.46	233096
Adult	29305	9768	9768	15	76.07	23.93	233099
Walking-activity	89599	29866	29866	5	14.73	0.61	233102
Phoneme	3242	1080	1080	6	70.65	29.35	233103
Skin-segmentation	147034	49011	49011	4	79.25	20.75	233104
Ldpa	98916	32972	32972	8	33.05	0.84	233106
Nomao	20679	6893	6893	119	71.44	28.56	233107
Cnae-9	648	216	216	857	11.11	11.11	233108
Blood-transfusion	448	149	149	5	76.20	23.80	233109
Bank-marketing	27126	9042	9042	17	88.30	11.70	233110
Connect-4	40534	13511	13511	43	65.83	9.55	233112
Shuttle	34800	11600	11600	10	78.60	0.02	233113
Higgs	58830	19610	19610	29	52.86	47.14	233114
Australian	414	138	138	15	55.51	44.49	233115
Car	1036	345	345	7	70.02	3.76	233116
Segment	1386	462	462	20	14.29	14.29	233117
Fashion-MNIST	42000	14000	14000	785	10.00	10.00	233118
Jungle-Chess-2pcs	26891	8963	8963	7	51.46	9.67	233119
Numerai28.6	57792	19264	19264	22	50.52	49.48	233120
Devnagari-Script	55200	18400	18400	1025	2.17	2.17	233121
Helena	39117	13039	13039	28	6.14	0.17	233122
Jannis	50239	16746	16746	55	46.01	2.01	233123
Volkert	34986	11662	11662	181	21.96	2.33	233124
MiniBooNE	78038	26012	26012	51	71.94	28.06	233126
APSFailure	45600	15200	15200	171	98.19	1.81	233130
Christine	3250	1083	1083	1637	50.00	50.00	233131
Dilbert	6000	2000	2000	2001	20.49	19.13	233132
Fabert	4942	1647	1647	801	23.39	6.09	233133
Jasmine	1790	596	596	145	50.00	50.00	233134
Sylvine	3074	1024	1024	21	50.00	50.00	233135
Dionis	249712	83237	83237	61	0.59	0.21	233137
Aloi	64800	21600	21600	129	0.10	0.10	233142
C.C.FraudD	170884	56961	56961	31	99.83	0.17	233143
Click Prediction	239689	79896	79896	12	83.21	16.79	233146

Table 9: Statistics on tabular datasets. Note that the OpenML ID denotes the ID used to retrieve the dataset (Gijsbers et al., 2019). Majority and Minority Class % shows the class imbalance within each dataset. For fair evaluation, we report balanced accuracy in all tabular experiments. # Feats. denotes the number of features in each dataset.